RSC Advances

PAPER

View Article Online
View Journal | View Issue

Cite this: *RSC Adv.*, 2025, **15**, 21408

Interaction of cardiomyocytes from CCND2-overexpressing human induced pluripotent stem cells with electrically conductive hydrogels†

Michelle Jang,‡[a] Yura Son,‡[b] Alejandra Patino-Guerrero,[b] Yamini Singh,[a] Keagan Neff,[a] Mehdi Nikkhah*[ac] and Wuqiang Zhu *[b]

The use of biomaterials has been widely studied as a platform to deliver regenerative cells, such as human induced pluripotent stem cells-derived cardiomyocytes (hiPSC-CMs), into damaged heart tissue. However, these biomaterials often lack the electroconductivity needed for effective heart function. In this study, we developed a gold nanorod-embedded gelatin-methacrylate (GelMA-GNR) hydrogel scaffold seeded with hiPSC-CMs and hiPSC-derived cardiac fibroblasts (hiPSC-CFs). Three experimental groups, pristine GelMA (GelMA), GelMA embedded with 0.5 mg mL^{-1} of GNRs (GelMA+0.5GNR), and GelMA embedded with 1.0 mg mL^{-1} of GNRs (GelMA+1.0GNR), were included in this study. hiPSC-CMs at 28 days after initiation of cardiogenic differentiation were used. The hiPSC-CMs (2.4 million) and hiPSC-CFs (0.4 million) were co-cultured on the GelMA hydrogel scaffold for 14 days before experiments to evaluate cell maturation. Morphological assessments through immunofluorescence staining showed enhanced alignment, sarcomere structure, and connexin-43 expression in the two GNR-treatment groups. GNRs did not affect cell viability or spontaneous beating but promoted the expression of maturation markers and improved action potential propagation modestly, as evaluated by reverse transcript PCR and optical mapping. In conclusion, these findings demonstrate that GNR-enhanced scaffolds facilitate hiPSC-CM maturation, offering a promising approach to improve the maturation of engineered heart tissue.

Received 29th April 2025
Accepted 19th June 2025

DOI: 10.1039/d5ra03024b

rsc.li/rsc-advances

1. Introduction

Myocardial infarction (MI), commonly referred to as a heart attack, is typically caused by the narrowing of coronary arteries which reduces blood flow and oxygen supply to the myocardium.[1] Due to the limited regenerative potency of adult cardiomyocytes, the loss of cardiomyocytes often results in the formation of fibrotic scar tissue, impairing contractility and electrical propagation of the heart and ultimately predisposing the heart to failure and arrhythmias.[2] The advent of human-induced pluripotent stem cells (hiPSCs) and their differentiation into cardiomyocytes (hiPSC-CMs) has brought significant advancements to cardiac regeneration and disease modeling. Despite these promising developments, critical challenges remain, including limited long-term survival, insufficient maturation, and inadequate coupling and alignment of grafted CMs with the host myocardium.[3–5] To overcome these obstacles, biomaterials such as polymeric scaffolds and hydrogels have been extensively explored for their ability to provide structural support and enhance the therapeutic efficacy of stem cells within three-dimensional (3D) environments.[6,7]

First-generation biomaterials, such as fibrin,[8,9] collagen,[10,11] alginate,[12,13] poly(*N*-isopropyl acrylamide) (PNIPAAm),[14] and poly(ethylene glycol) (PEG)-based copolymers,[15] have demonstrated their utility in supporting cellular spreading, viability and differentiation. However, these biomaterials lack the electroconductive properties necessary to support electrical signal propagation among cardiomyocytes.[16] Consequently, there has been a growing emphasis on developing electroconductive biomaterials to emulate the conductive microenvironment of healthy myocardium.[16–18] To date, various conductive components, such as carbon-based materials (*i.e.*, carbon nanotubes, ribbons, and reduced graphene oxide),[19–23] gold nanomaterials (*i.e.*, gold nanorods and gold nanowires),[18,24,25] as well as electroconductive polymers (*i.e.*, polyaniline),[17,26] have been integrated into scaffolding biomaterials to generate a functional and conductive cardiac tissue resemble native myocardium. Among these, gold nanomaterials have gained attention due to their biocompatibility, stability, ease of fabrication, and robust electroconductive properties.[27]

[a]*School of Biological and Health Systems Engineering, Arizona State University, Tempe, AZ 85287, USA. E-mail: Mehdi.Nikkhah@asu.edu*

[b]*Department of Cardiovascular Medicine, Physiology and Biomedical Engineering, Center for Regenerative Biotherapeutics, Mayo Clinic, Scottsdale, AZ 85259, USA. E-mail: Zhu.Wuqiang@mayo.edu*

[c]*Biodesign Virginia G. Piper Center for Personalized Diagnosis, Arizona State University, Tempe, AZ 85287, USA*

† Electronic supplementary information (ESI) available. See DOI: https://doi.org/10.1039/d5ra03024b

‡ These authors contributed to the work equally.

In our recent studies, we demonstrated that embedding gold nanorods (GNRs) in gelatin methacrylate (GelMA) hydrogels (*i.e.*, GelMA-GNR) improved the functionality and maturation of both rat-derived CMs[28–30] as well as hiPSC-CMs, as evidenced by enhanced sarcomere organization, synchronous calcium flux, and increased calcium transient intensity.[31,32] Additionally, we have reported that hiPSC-CMs overexpressing cyclin D2 (hiPSC-CCND2^{OE}CMs) exhibited significantly increased proliferation and improved graft integration with the host myocardium after transplantation into MI-induced mice.[33] Building on these findings, in this current study, we combined hiPSC-CCND2^{OE}CMs with electrically conductive GelMA-GNR hydrogels synergistically to enhance the formation, structural organization and functionalities of engineered heart tissue (EHT). We seeded GelMA-GNR hydrogels with a co-culture of hiPSC-CCND2^{OE}CMs and hiPSCs-cardiac fibroblast cells (hiPSC-CFs) and comprehensively assessed structural organization, function and gene expression of the engineered cardiac tissue. Overall, the current study aimed to bridge critical gaps in cardiac tissue engineering by integrating innovative biomaterials and advanced cell engineering to improve cardiac regeneration outcomes.

2. Materials and methods

2.1 GelMA fabrication

GelMA was synthesized following a previously established protocol.[34] In short, gelatin (10% w/v) (G1890-500G, Sigma Aldrich, St. Louis, MO, USA) was dissolved in phosphate buffer saline (PBS) (P3813, Sigma Aldrich) at 50 °C with vigorous stirring for about 1 hour or until fully dissolved. While stirring, methacrylate anhydride (MA) (0.8 mL g^{-1} of used gelatin) (276685-550ML, Sigma Aldrich) was slowly added to the gelatin mixture and vigorously stirred at 50 °C for an addition 3 hours. Once the mixture was stirred homogenously, the solution was aliquoted into 50 mL conical tubes and centrifuged for 3 minutes at 3500 g at room temperature to remove any unreacted MA. The clear solution was decanted into a glass beaker and diluted with two volumes of prewarmed PBS (40 °C) and maintained at 40 °C. While stirring, the solution was transferred into a dialysis membrane (12 kDa MWCO) and dialyzed against deionized (DI) water. The water was changed twice a day for 7 days. The pH of the solution was then adjusted using 1 M $NaHCO_3$. After adjusting the pH, the solution was filtered through a 0.2 μm filter and aliquoted into 50 mL conical tubes and kept at −80 °C overnight. The frozen GelMA solution was either kept at −80 °C until future use or lyophilized for 7 days and stored at −20 °C for use.

2.2 Gold nanorod synthesis

Two main components are involved in GNR synthesis: seed solution and growth solution. The seed-mediated growth method, as described previously,[35] was adapted with some modifications. First, to prepare the seed solution, 2 mL of cetyltrimethylammonium bromide (CTAB, 0.2 M, 30 °C) was combined with 2 mL of $HAuCl_4$ (0.5 mM, 30 °C) while stirring continuously, which resulted in a deep yellow color. While the combined solution was stirred gently, 240 μL of ice-cold $NaBH_4$ (0.01 M) was added, followed by vigorous vortexing at room temperature for 2 minutes, which led to a color change to light brown. To ensure complete reduction of $NaBH_4$, the seed solution was left undisturbed for 1.5 hours at 30 °C. The second component, the growth solution, was prepared by adding 1 mL of $AgNO_3$ (0.0045 M, 30 °C) to 20 mL of CTAB solution (0.2 M, 30 °C) and gently inverting the mixture several times. The concentration of $AgNO_3$ in the growth solution has been optimized to aid in achieving a high yield reaction with narrow size distribution, and to reduce batch-to-batch variation in the synthesis of the GNRs, as reported previously.[35–37]

Then, 20 mL of $HAuCl_4$ (1 mM, 30 °C) was added to the existing mixture and inverted gently until the solution became homogenous, resulting in a deep yellow color. Next, 280 μL of ascorbic acid (0.0788 M, 30 °C) was added and inverted gently immediately, turning the solution colorless. Finally, 48 μL of seed solution (30 °C) was added to the growth solution and kept for 24 hours at 30 °C. After 24 hours, the GNR solution was transferred into Eppendorf tubes and centrifuged at 13.8 g for 10 minutes. The supernatant was discarded while leaving the formed pellet untouched. The pellets from each Eppendorf tube were combined into a single Eppendorf tube, resuspended in 500 μL of PBS, and centrifuged for 9.6 g for 15 minutes. After discarding the supernatant, the GNR pellet was resuspended in 150 μL PBS and stored at room temperature for future use.

2.3 Gold nanorod size measurement

The synthesis of GNRs followed a method similar to the previously established work, using the same standard curve equation to calculate the gold content in the GNR solution for this study.[31] The ultraviolet-visible-near-infrared (UV-vis-NIR) extinction spectra, ranging from 300 to 990 nm in 10 nm increments, were measured using a spectrophotometer (BioTek Synergy H1 Plate Reader, BioTek Instruments, Inc., Winooski, VT, USA) to study the surface plasmon resonance (SPR) of the synthesized GNRs. Transmission electron microscopy (TEM) characterization of the GNRs was also performed using a TEM/Scanning transmission electron microscopy (STEM) (Titan 300/80, FEI, Hillsboro, OR, USA) at an operating voltage of 200 kV. TEM images were analyzed with ImageJ software to measure the diameter and length of the GNRs.

2.4 3-(Trimethoxysilyl)propyl methacrylate (TMSPMA) treatment of glass slides

The preparation of TMSPMA-treated glass slides was conducted over a three-day process. On the first day, 50 g of NaOH pellets (VWR Inc., Randor, PA, USA) were dissolved in 450 mL of DI water under a fume hood. Glass slides (16004-308, VWR Inc.) were then placed in the solution in a staggered arrangement to ensure full surface contact with the NaOH solution. The slides were left in the solution overnight. On the second day, the NaOH was discarded, and the glass slides were thoroughly rinsed individually with DI water. The rinsed slides were subsequently immersed in three consecutive 100% ethanol

baths for 5 minutes each and then air dried. Once dry, the slides were wrapped in aluminum foil and baked at 80 °C for 1 hour. After baking, 5 mL of TMSPMA was applied evenly across the stacked glass slides using a syringe under a fume hood to ensure uniform coating. The slides were then baked overnight at 80 °C. On the final day, the coated slides were cleaned in three consecutive baths of 100% ethanol, air dried, wrapped with aluminum foil, and baked again for 1 to 2 hours at 80 °C. The completed TMSPMA-coated glass slides were stored at room temperature for future use.

2.5 Synthesis of GNR-embedded conductive GelMA hydrogels

Three experimental groups were prepared: (1) pristine GelMA (GelMA), (2) GelMA embedded with 0.5 mg mL^{-1} of GNRs (GelMA+0.5GNR), and (3) GelMA embedded with 1.0 mg mL^{-1} of GNRs (GelMA+1.0GNR). The synthesized GNRs were first centrifuged at 9.6 g for 15 minutes, and then the pellets were resuspended in 150 μL of 3% GelMA and sonicated in a 60 °C water bath for 1 hour. Meanwhile, 2-hydroxy-1-(4-(hydroxyethoxy)phenyl)-2-methyl-1-propanone (Irgacure 2959, Sigma Aldrich) as a photoinitiator (1.0% w/v) was dissolved in PBS and filtered using a 0.2 μm membrane. The appropriate amounts of GNRs (0.5 and 1.0 mg mL^{-1}) were added to the GelMA prepolymer solution. The final prepolymer solution contained 0.5% w/v of Irgacure 2959 and 15% w/v of GelMA prepolymer solution, and the respective concentrations of GNRs. The mixtures were then sonicated in a 60 °C water bath for 1 hour. After sonication, hydrogel scaffolds with a thickness of 150 μm were synthesized.

To fabricate the hydrogel construct, 16 μL of the prepolymer solution was dropped onto a Claritex Supa Mega Slide (MAC-1400-02A, CellPath Ltd., Powys, United Kingdom). A TMSPMA-coated glass slide (1.5 cm × 1.5 cm) equipped with 150 μm thick spacers at three corners was placed on top of the prepolymer droplet to spread the solution evenly. The films were UV-crosslinked using a UV source (360–480 nm) positioned 8 cm above the hydrogel films, providing an intensity of approximately 7.64 mW cm^{-2}. Crosslinking was conducted for 50 seconds for all experimental conditions. The resulting hydrogel films were then submerged in RPMI 1640 medium with penicillin/streptomycin overnight.

2.6 hiPSC culture and cardiogenic differentiation

The culture and cardiogenic differentiation of hiPSCs-CMs were performed following an established protocol.[38,39] Briefly, hiPSC line (DF-19-9-7T) was purchased from WiCell Research Institute Inc. and transfected with the human CCND2 gene under the control of α-MHC promoter.[39] Cells were cultured on Matrigel (354230, Corning, Corning, NY, USA)-coated 6-well plates with mTeSR Plus medium (100-0276, Stem Cell Technologies, Vancouver, Canada) at 37 °C with 5% CO_2. Once the hiPSCs reached 70–80% confluency, differentiation into cardiomyocytes was initiated. On day 1 of differentiation, cells were treated with 6 μm CHIR99021 (4423, BioGems, Westlake village, CA, USA) in RPMI 1640 medium (11875-085, Gibco, Grand Island, NY, USA) with 2% of B27 minus insulin (A1895601, Gibco) with a total volume of 3 mL per well. On day 2, 2 mL of RPMI 1640 + B27 minus insulin was added to each well. The next day (day 3), 1 mL of RPMI 1640 + B27 minus insulin was added. On day 4, the old media was removed, and the cells were washed with PBS. Then, 3 mL of RPMI 1640 + B27 minus insulin medium supplemented with 3 μM of IWR1 (1128234, BioGems) was added to the wells, and this medium was replaced every 48 hours. On day 9, the medium was switched to RPMI 1640 supplemented with 2% B27 (17504044, Gibco). Once differentiation into cardiomyocytes was achieved, the purification process was carried out using glucose-free RPMI 1640 medium (11879020, Gibco) supplemented with 2% B27 and a 4 mM sodium DL-lactate solution (L4263-500ML, MilliporeSigma, Rockville, MD, USA) for 72 hours.

2.7 Cardiac fibroblasts differentiation

The differentiation of hiPSCs into cardiac fibroblasts (hiPSC-CFs) was performed according to a previously established protocol.[31] hiPSCs (IMR90-4, WiCell Research Institute Inc.) were treated with 1 mL of 0.5 mM EDTA per well and incubated for approximately 6 minutes to facilitate cell dissociation. The dissociated cells were then replated onto Matrigel-coated 6-well plates at a density of 0.1–0.15 million cells per well in mTeSR1 medium, with the medium replaced daily. Once the cells reached 80–90% confluency, differentiation into cardiac fibroblasts was initiated. On day 1, the existing medium was removed, and the cells were treated with 4 mL of RPMI 1640 medium supplemented with B27 minus insulin and 7 μM CHIR99021. After 24 hours (day 2), the medium was replaced with 5 mL of RPMI 1640 supplemented with B27 minus insulin. On day 3, the old medium was removed, and 2.5 mL of cardiac fibroblast differentiation medium (hCFBM) supplemented with 70 ng μL^{-1} basic fibroblast growth factor (bFGF) was added to each well and incubated for 48 hours at 37 °C with 5% CO_2. After day 5, the hCFBM medium supplemented with 70 ng μL^{-1} bFGF was refreshed every other day until day 20. After day 20, the differentiated hiPSC-CFs were either cryopreserved or passaged and maintained in fibroblast growth medium 3 (FGM3, C-23025, PromoCell, Heidelberg, Germany).

2.8 Development of engineered cardiac tissue

To form cardiac tissues, 60 μL of a cell suspension containing 0.4 million hiPSC-derived CCND2 overexpressing cardiomyocytes (hiPSC-$CCND2^{OE}$CMs) and hiPSC-CFs (6 : 1 ratio) was carefully deposited (seeded) onto a thin layer (150 μm) of GelMA, GelMA + 0.5GNR, and GelMA + 1.0GNR hydrogel scaffolds. The scaffolds were incubated at 37 °C for approximately 2.5 hours to facilitate cell attachment to the hydrogel surface. After incubation, 1.5 mL of medium supplemented with insulin was gently added to each well to fully immerse the hydrogel scaffolds. The cultures were maintained for 14 days, with the medium replaced every other day to ensure optimal cell growth and scaffold stability.

2.9 Cell viability

Cardiac tissues were evaluated for cell viability on 3 post-seeding using a Live/Dead Assay kit (30002-T, Biotium, Fremont, CA, USA). The kit consisted of calcein-AM (Cl-AM) and ethidium homodimer III (EthD-III). A Live/Dead solution was prepared by diluting 4 mM Cl-AM and 2 mM of EthD-III in 3 mL of warm PBS in a 1 : 4 ratio. Culture medium was removed from the well plates, followed by two washes with PBS, each with a 5 minutes incubation at room temperature. Subsequently, 1 mL of Live/Dead solution was added to each well, and the plates were incubated for 25 minutes at room temperature, protected from light. After incubation, cardiac tissues were washed three times with PBS for 5 minutes. Z-stack fluorescent images of live (green) and dead (red) cells were captured at 10× magnification using a modular inverted light microscope (DMi8, Leica Microsystems, Germany).

2.10 Immunofluorescence staining

On day 14 of culture, cardiac tissues were washed with PBS and fixed with 4% paraformaldehyde for 15 minutes at room temperature. After fixation, the samples were washed twice with PBS containing glycine (0.1 M) for 10 minutes each, followed by a single wash with PBS containing 0.05% Tween-20 for 10 minutes at room temperature. Permeabilization was performed by incubating the samples in 1% Triton-X-100 in PBS for 30 minutes at room temperature. For Ki67 staining, antigen retrieval was carried out by immersing the samples in 10 mM citrate buffer solution at 94 °C for 10 minutes, followed by cooling at room temperature for 30 minutes. Samples were then blocked with 10% goat serum in PBS containing 0.05% Tween-20 for 1 hour at room temperature. Primary antibodies were diluted in 10% goat serum, and the samples were incubated overnight at 4 °C. The primary antibodies used for this study include Alexa Fluor 488 Phalloidin (1 : 1000), mouse monoclonal anti-integrin β1 (1 : 100), rabbit monoclonal anti-vimentin (1 : 100), mouse monoclonal anti-TroponinT (TnT) (1 : 100), mouse monoclonal anti-sarcomeric alpha-actinin (1 : 100), rabbit polyclonal anti-connexin43 (1 : 100), and rabbit polyclonal ki67 (1 : 300). After incubation with primary antibodies, the samples were washed five times with PBS containing 0.05% Tween-20 at room temperature. Secondary antibodies were diluted in 10% goat serum in PBS containing 4′,6-diamidino-1-phenylindole (DAPI, 1 : 1000) and incubated for 1 hour at room temperature. The secondary antibodies used include Alex Fluor 647 goat anti-mouse (1 : 400), Alexa Fluor 488 goat anti-mouse (1 : 400), Alexa Fluor 647 goat anti-rabbit (1 : 400), and Alexa Fluor 488 goat anti-rabbit (1 : 400). The samples stained for F-actin/Integrin, vimentin/cardiac troponin T (cTnT), Ki67/cTnT, and connexin-43 (Cx43)/α-actinin were imaged using a Leica SP8 White Light Laser Confocal microscope with Light Sheet at 20× and 63× magnifications. Z-stack images were captured and processed using ImageJ software.

2.11 Assessment of sarcomere striation

To evaluate the sarcomere quality (coverage and striation) of the EHTs formed on the hydrogel scaffolds, a scoring metric based on immunofluorescence images of sarcomeric α-actinin was employed as described in previous studies.[31,40] In this method, immunofluorescence images were divided into nine equal sections. Each section was assessed for sarcomere quality on a scale from 0 (lowest) to 10 (highest), with the scores reflecting the presence, alignment, and organization of sarcomeres within the tissue. The qualitative scores for all nine sections of each image were averaged to calculate the sarcomere striation quality for that specific image. Subsequently, the average values for each biological replicate were computed. Finally, the aggregated sarcomere striation quality across all biological replicates was determined by averaging the replicate values providing a comprehensive assessment of sarcomere organization within the cardiac tissues.

2.12 Spontaneous beating behavior analysis of cardiac tissues

The spontaneous beating behavior of the EHTs was evaluated following established protocols.[41–43] Briefly, EHTs were imaged using a fluorescence microscope (DMi8, Leica Microsystems) equipped with a 20× objective. Time-lapse images were captured for 20 seconds on days 7 and 14 of culture. Key parameters, including beating patterns, beats per minutes (BPM), interbeat interval variability (IIV), contraction amplitude, and relaxation time, were analyzed using MUSCLEMOTION, an open software tool specifically designed for quantitative assessment of contractile behaviors in cardiac tissues.[44,45]

2.13 Gene expression analysis

Reverse transcription quantitative polymerase chain reaction (RT-qPCR) was conducted to quantify the relative expression levels of cardiac-specific genes. Samples from the experimental groups (GelMA, GelMA+0.5GNR, and GelMA+1.0GNR) were collected on day 14 of culture. GelMA group was used for gene expression normalization. Cells were enzymatically dissociated by adding prewarmed TrypLE™ Select Enzyme (A1217701, Gibco) for 10–15 minutes at 37 °C, followed by neutralization with RPMI 1640 supplemented with 2% B27 medium. The dissociated cells were transferred to 15 mL falcon tubes, centrifuged at 300 g for 4 minutes, and resuspended in 1 mL PBS. After a second centrifugation (300 g, 3 minutes), the supernatant was discarded, and the cell pellets were lysed in 350 μL of lysis buffer.

RNA extraction was performed using the Quick-RNA Micro-Prep Kit (R1050, Zymo Research, Irvine, CA, USA) according to the manufacturer's protocol. RNA purity and concentration were evaluated *via* A260/280 and A260/230 nm absorbance ratios measured with a Nanodrop One instrument (Thermo Scientific, Waltham, MA, USA). cDNA synthesis was carried out using the qScript cDNA Supermix (95048-100, Quantabio, Beverly, MA, USA). RT-qPCR was performed using iTaq Universal SYBR Green Supermix (1725121, Bio-Rad, Hercules, CA, USA) with validated primers for ACTNT2, GJA1, MYH6, MYH7, TNNT2, TNNI3, MLC2V, MLC2A, ATP2A2, CASQ2, S100A1, and 18S as described in our previous study (Table S2†).[31] Gene expression was normalized to 18S as internal control. Relative expression levels were calculated using the 2-ΔΔCT method. Relative fold changes in gene expression were analyzed and

using GraphPad Prism software, including heatmaps generated from row *Z*-scores for each gene.

2.14 Optical mapping

For the electrophysiological characterization of the EHTs a custom setup was utilized. The imaging system consisted of a CMOS sensor (sensor size: 17.6 × 10.4 mm MiCAMO3-N256) controlled by a computer software (BV Workbench 2.7.2), excitation filter (466 nm), dichroic mirror (Edge 500 nm), emission filter (525 nm), and LED light source with shutter (LEX9, 460 nm). Additionally, the CMOS sensor was coupled with a combination of an 85 mm lens (Samyang 1.4/85 mm) and a 1.0× objective lens (LEICA plan APO 1.0×) to form a field of view of 10.4 × 10.4 mm. To facilitate the recording of the electrophysiological activity of the tissues, the samples were treated with the FluoVolt Membrane Potential dye (F10488, ThermoFisher Scientific, Waltham, MA, USA). Briefly, the FluoVolt dye (component A) was dissolved in a Modified Tyrode's solution (1 : 1000), the samples were washed twice with the Tyrode's solution before replacing it with the FluoVolt solution. The EHTs were incubated for 20 minutes at 37 °C and then washed twice with the Tyrode's buffer. The tissues were placed in a 35 mm Petri dish submerged into superficial-perfused Tyrode's solution at 37 °C with carbogen for signal recording.

The baseline electrophysiological activity of each of the samples was recorded for 8 seconds. Then, point stimulation was formed by placing silver leads at the edge of the EHT to deliver S1–S1 pacing at 1.8, 2.0, 2.5, and 3.0 Hz, from 3 to 5 V in 0.5 V increments. The obtained videos were processed using the BV Workbench software. The signals were filtered using a mean filter, a drift removal filter, and a low-pass filter (cut-off: 40 Hz). Finally, the conduction velocity (CV) and action potential durations at 50% and 80% repolarization (APD50 and APD80, respectively) were calculated utilizing built-in features of the software. A *Z*-score heat map for the CV was constructed $\left(Z = \frac{\text{observed value} - \text{mean of the sample}}{\text{standard deviation of the sample}}\right)$.

2.15 Statistical analysis

Unless otherwise specified, all experiments were conducted with four biological replicates. Quantitative analyses were performed using GraphPad Prism software (GraphPad Prism v.6), with data presented as means ± standard deviation (S.D). To assess significant differences among experimental conditions, one-way ANOVA with Tukey's posthoc was used for analyzing cell viability, optical mapping, and immunofluorescence staining cell coverage. For spontaneous beating behavior analysis, two-way ANOVA was performed, *p*-value of less than 0.05 was considered statistically significant.

3. Results

3.1 Fabrication of GNRs-Embedded GelMA hydrogel scaffolds

GelMA-GNR hydrogel scaffolds were fabricated one day before culturing the cardiac cells and immersed in RPMI 1640 medium with 3% penicillin/streptomycin overnight to prevent contamination, and no contamination was observed in any of the cultures throughout the course of the experiments. The schematic workflow is depicted in Fig. 1A. This summarizes the multi-step process beginning with the synthesis and characterization of GNRs, followed by the fabrication of GNR-embedded GelMA hydrogel scaffolds, and culminating in the formation and functional assessment of EHTs using gene-edited hiPSC-CCND2^{OE}CMs and hiPSC-CFs. GNRs were synthesized using a seed-mediated growth method and characterized by UV-vis spectroscopy (Fig. 1B), which revealed distinct transverse (520 nm) and longitudinal (730 nm) surface plasmon resonance (SPR)

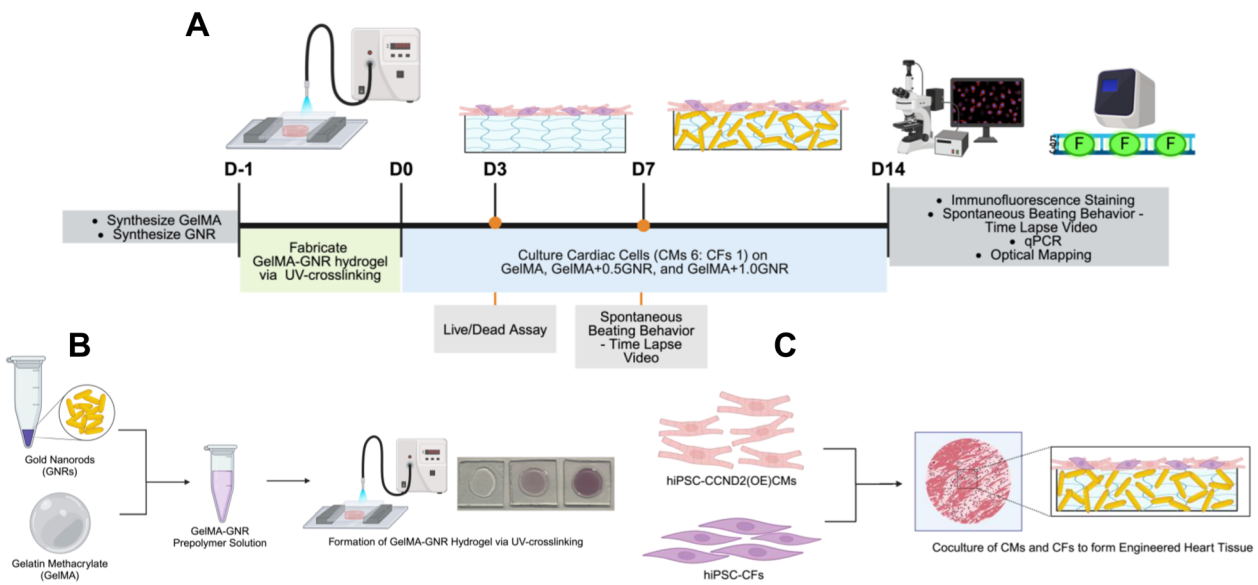

Fig. 1 Schematic workflow of the study design. (A) Experimental workflow of the study. (B) Fabrication process of the gold nanorods-embedded GelMA hydrogel (GelMA-GNR). (C) Formation of engineered cardiac tissue on top of the GelMA-GNR (created with BioRender).

peaks (Fig. S1A†), confirming successful formation. TEM imaging further confirmed the morphology of the GNRs (Fig. S1B†), revealing elongated rod-like structures with an average length of 50.9 ± 7.7 nm, diameter of 16.7 ± 3.7 nm, and an aspect ratio of 2.7 (Fig. S1C and D†). Three experimental conditions were used in this study: (1) GelMA (control), (2) GelMA with 0.5 mg mL^{-1} of GNRs (GelMA+0.5GNR), and (3) GelMA with 1.0 mg mL^{-1} of GNRs (GelMA+1.0GNR). For each sample, 16 μL of GelMA or GelMA-GNR prepolymer solution was dropped onto 1.5 cm square TMSPMA glass slides with a spacer thickness of 150 μm and crosslinked under UV light for 50 seconds. A co-culture of hiPSC-CCND2^{OE}CMs and hiPSC-CFs was seeded onto the surface of the GelMA-GNR scaffolds at a 6 : 1 ratio and cultured for 14 days (Fig. 1C).

3.2 Cardiac tissue viability

To evaluate the effect of co-culturing hiPSC-CCND2^{OE}CMs and hiPSC-CFs, as well as the incorporation of GNRs, on cell attachment to GelMA/GelMA-GNR hydrogel scaffolds, hiPSC-CCND2^{OE}CMs were cultured both as mono-cultures and co-cultures with hiPSC-CFs. All EHTs were maintained in culture for 14 days, and 3 × 3 tile images were captured on day 3, 7, and 14 using a 20× objective for all experimental conditions. Mono-cultured EHTs exhibited significant cell detachment, with most hiPSC-CCND2^{OE}CMs forming isolated aggregates without interconnectivity (Fig. S2†). Conversely, co-cultured EHTs presented improved cell attachment and a more uniform distribution of cells across the hydrogel surface. Consequently, all subsequent experiments were performed using co-cultures of hiPSC-CCND2^{OE}CMs and hiPSC-CFs.

Cell viability was measured on day 3 after cell seeding using a Live/Dead assay (Fig. S3†). Cell viability staining showed no difference among the groups (Fig. S3A†), and the quantification results indicated no significant differences in cell survival across the experimental groups: GelMA (96.2 ± 2.1%), GelMA+0.5GNR (96.6 ± 1.5%), and GelMA+1.0GNR (96.8 ± 1.1%) ($n = 4$ for each group) (Fig. S3B†). These findings suggest that GelMA and varying GNR concentrations did not adversely affect cellular viability.

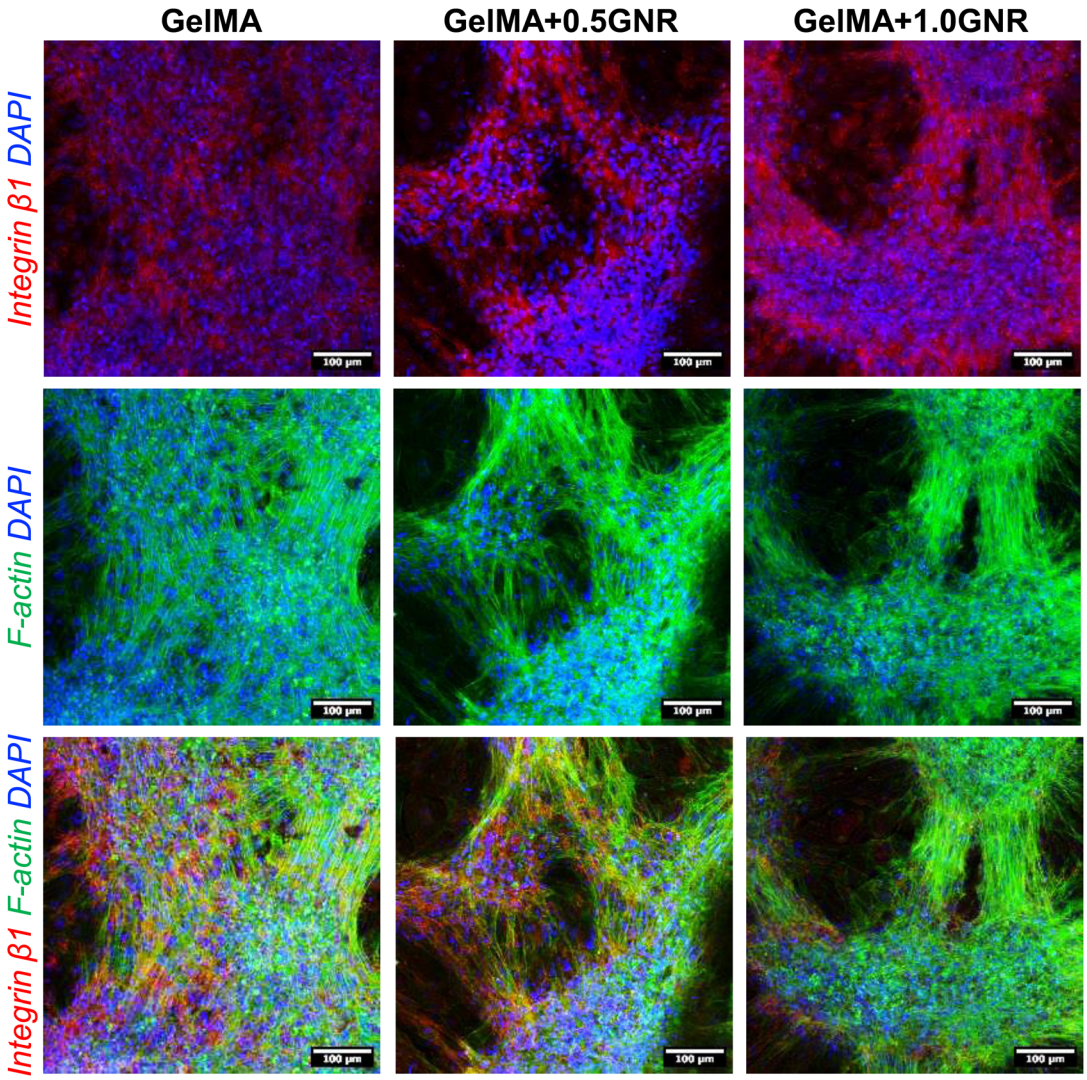

Fig. 2 Structural assessment of the of cardiac tissues. Immunofluorescence (IF) staining images of cardiac tissues formed on GelMA, GelMA+0.5GNR, and GelMA+1.0GNR for 14 days stained for Integrin β1 (red), F-actin (green), and nuclei (blue). Scale bar: 100 μm.

3.3 Assessment of cardiac tissue formation

To examine the formation and phenotype of EHTs on these nanoengineered electroconductive hydrogels, GelMA and GelMA-GNR scaffolds were stained with F-actin and integrin β1 (Fig. 2). Immunofluorescence images revealed that cells within the EHTs exhibited a similar morphology across all experimental groups. However, the incorporation of GNRs appeared to promote clustering of CMs.

To further investigate the spatial distribution and organization of hiPSC-CCND2^{OE}CMs and hiPSC-CFs within the EHTs, GelMA and GelMA-GNR samples were further stained for cardiac troponin T (cTNT), a marker for CMs, and vimentin, a marker for CFs (Fig. 3). The results demonstrated that the addition of GNRs enhanced the local alignment of both hiPSC-CCND2^{OE}CMs and hiPSC-CFs, specifically on connection areas between the cellular clusters. Notably, in the GelMA+1.0GNR group, hiPSC-CFs were evenly distributed throughout the cardiac tissue, indicating improved overall tissue organization compared to the GelMA and GelMA+0.5GNR groups.

3.4 Evaluation of proliferative potential of hiPSC-CCND2^{OE}CMs on GelMA/GNR hydrogel scaffolds

The overexpression of the cell cycle activator Cyclin D2 (CCND2) in hiPSC-CMs has been demonstrated as a potent approach to enhance the proliferation of these cells.[46] To that end, we further assessed the proliferative potential of the hiPSC-CCND2^{OE}CMs cultured on GelMA-GNR hydrogel scaffolds. The samples were co-stained with Ki67, a marker for cell proliferation, and cTnT, a marker for cardiomyocytes (Fig. 4). Immunofluorescence staining revealed evidence of hiPSC-CM proliferation across all experimental groups.

3.5 Expression of cardiac-specific proteins

To further characterize the phenotype of EHTs, immunofluorescence staining was performed using cardiac-specific markers, specifically Cx43 and sarcomeric α-actinin across all samples (Fig. 5). Cx43 is a gap-junction protein essential for mediating electrical coupling between cardiac cells, while α-

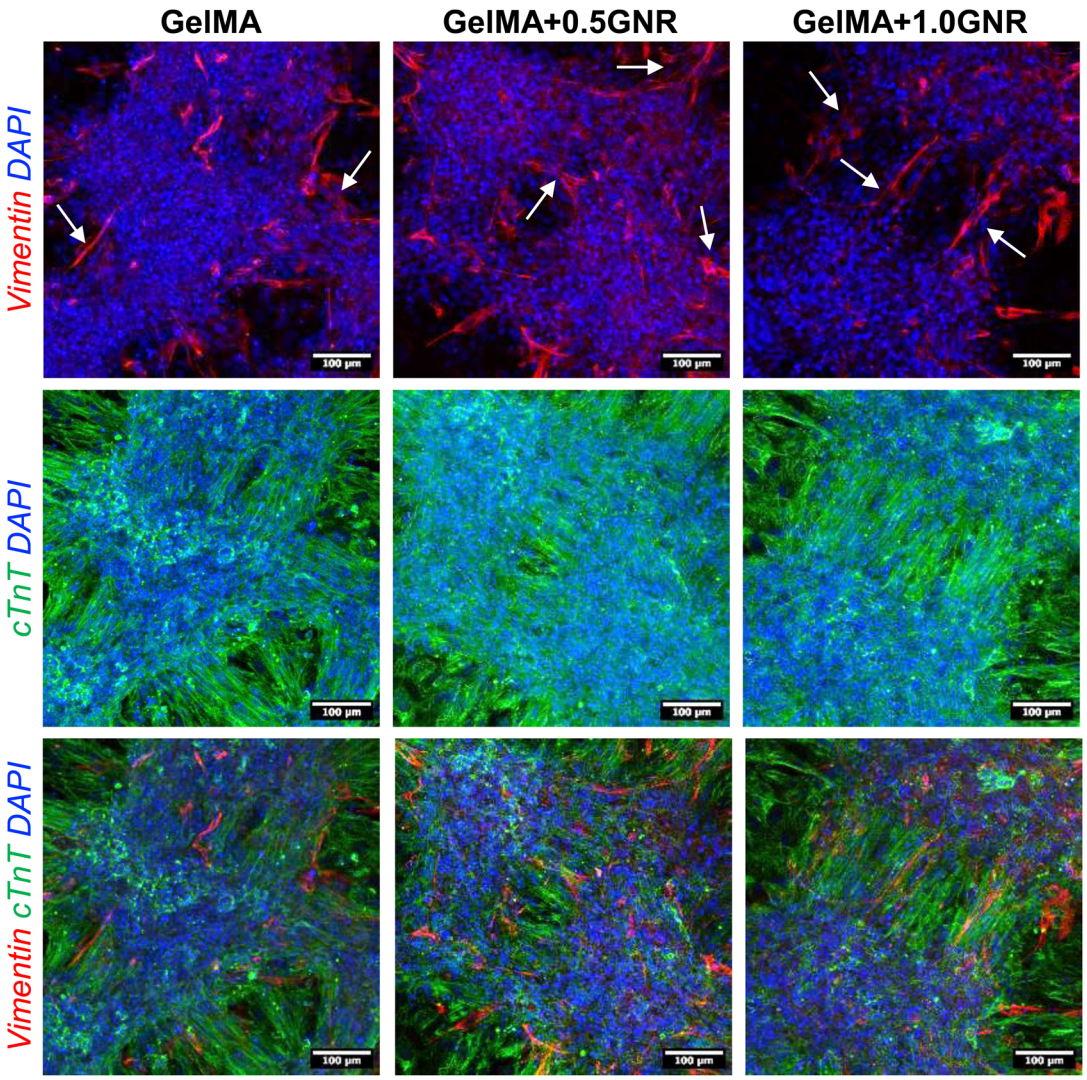

Fig. 3 Distribution of cardiac cells. IF staining images of cardiac tissues formed on GelMA, GelMA+0.5GNR, and GelMA+1.0GNR for 14 days stained for Vimentin (red), cTnT (green), and nuclei (blue). Scale bar: 100 μm.

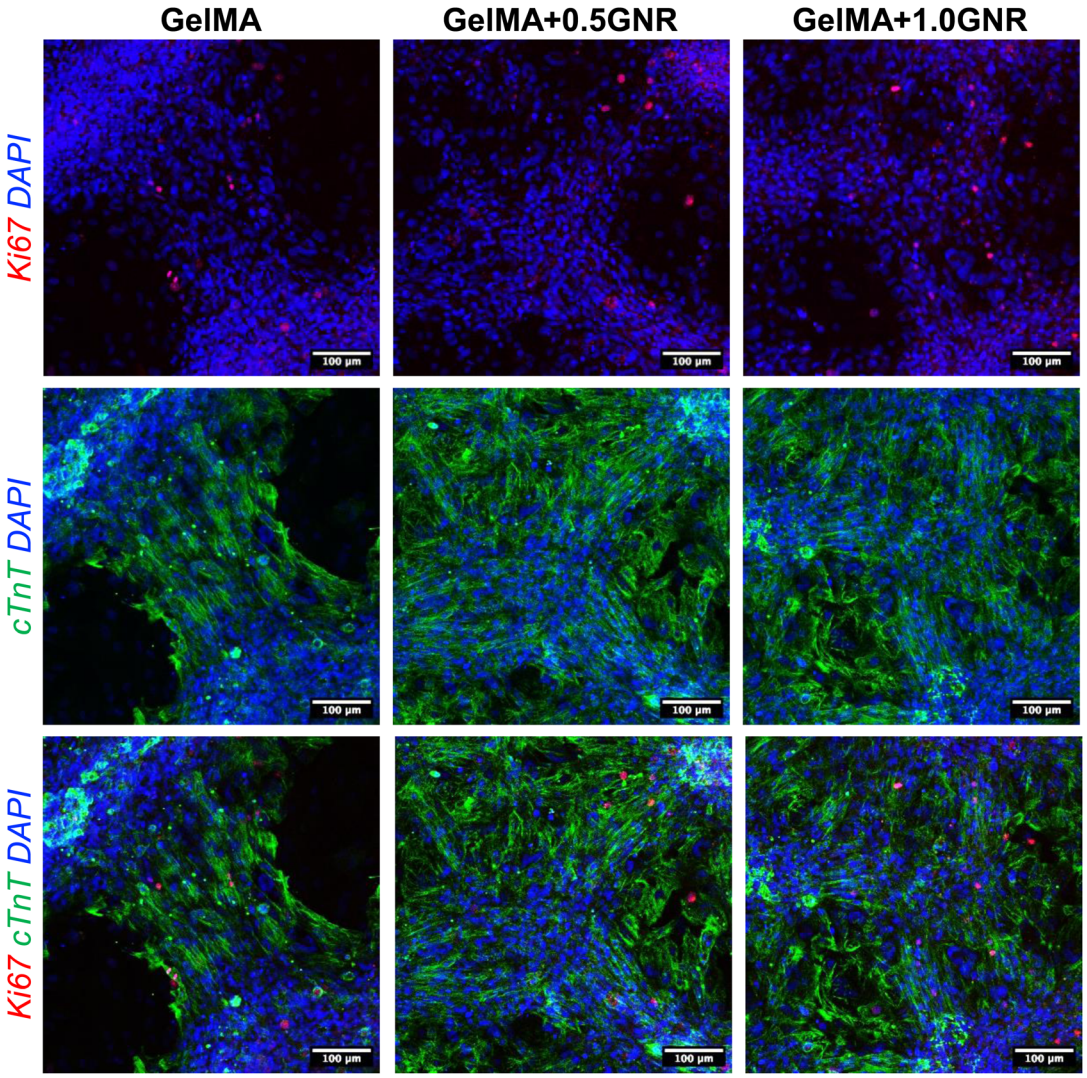

Fig. 4 Proliferative potency of hiPSC-CCND2^{OE}CMs. Immunofluorescence (IF) staining images of cardiac tissues formed on GelMA, GelMA+0.5GNR, and GelMA+1.0GNR for 14 days stained for ki67 (red), cTnT (green), and nuclei (blue). Scale bar: 100 μm.

actinin is a sarcomeric protein localized at the Z-disks, crucial for structural organization. Immunofluorescent analysis demonstrated increased expression and organization of striated sarcomeric α-actinin and Cx43 in hiPSC-CCND2^{OE}CMs cultured on GelMA-GNR hydrogel scaffolds as compared to GelMA alone (Fig. 5A). Quantitative analysis revealed a significant increase in Cx43 area coverage in the GelMA+0.5GNR (0.11423821 ± 0.0319044 Pix^2) and GelMA+1.0 GNR groups (0.05470512 ± 0.00997791 Pix^2) compared to the GelMA alone group (0.02420539 ± 0.00675354 Pix^2) (Fig. 5B). Furthermore, sarcomere quality was assessed *via* qualitative scoring, showing enhanced sarcomere striation in GelMA-GNR groups, particularly in the GelMA+0.5GNR condition (Fig. 5C). These findings are consistent with our prior research, where the incorporation of electroconductive components into hydrogel scaffolds promoted the development of organized, striated cardiac tissues.[31]

3.6 Gene expression analysis

As there were changes in structural organization of the EHTs with the incorporation of the GNRs, observed through immunofluorescence staining, RT-qPCR was performed to assess changes induced at gene expression level. Specifically, we assessed and quantified the expression of genes related to the cellular and tissue ultrastructure (MYH7, MYH6, TNNT2, TNNI3, MLC2V, MLC2A, GJA1, and ACTN2) as well as calcium handling genes (CASQ2, S100A1, and ATP2A2). On the day of the experiment (day 0), 6 : 1 ratio of CMs and CFs were cultured on GelMA, GelMA+0.5GNR, and GelMA+1.0GNR hydrogels and all the conditions were cultured for 14 days (Fig. 6A). While no significant differences were observed in the gene expression levels (Fig. S4†), based on the *Z*-score heatmap (Fig. 6B), compared to the GelMA group, there was a trend towards an overall increased expression of the assessed genes in the EHTs formed on the GelMA-GNR hydrogel scaffolds, specifically GelMA+1.0GNR condition.

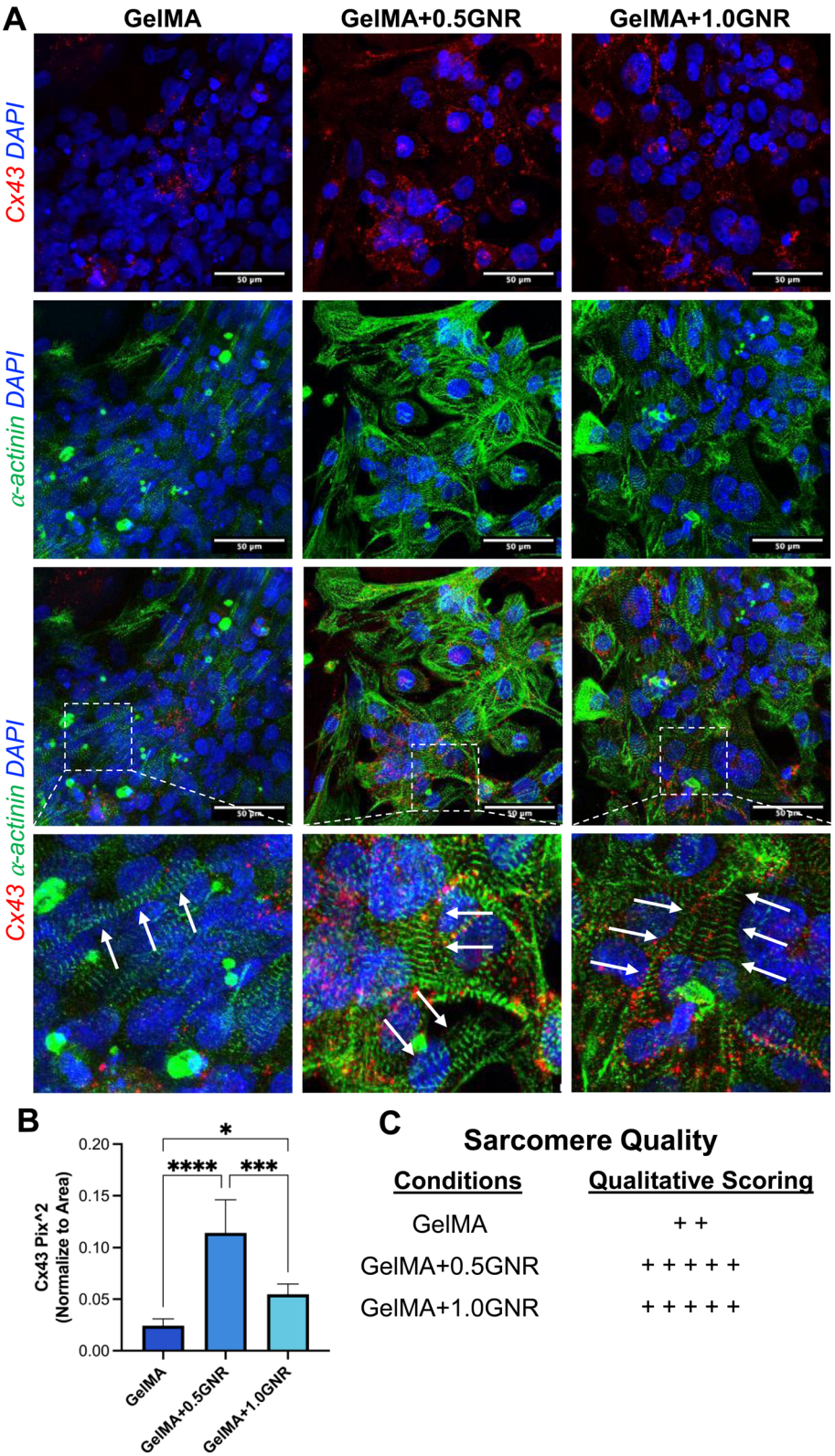

Fig. 5 Contractile integration of EHTs *via* cardiac-specific markers. (A) IF staining images of cardiac tissues formed on GelMA, GelMA+0.5GNR, and GelMA+1.0GNR for 14 days stained for Cx43 (red), α-actinin (green), and nuclei (blue). Scale bar: 50 μm. (B) Cell coverage analysis of the EHTs measured by Cx43 (one-way ANOVA with a Tukey's posthoc test, $n = 4$). Data was expressed as mean ± standard deviation. *$p < 0.05$, ***$p < 0.001$, ****$p < 0.0001$, and ns (not significant). (C) Qualitative scoring of sarcomere quality.

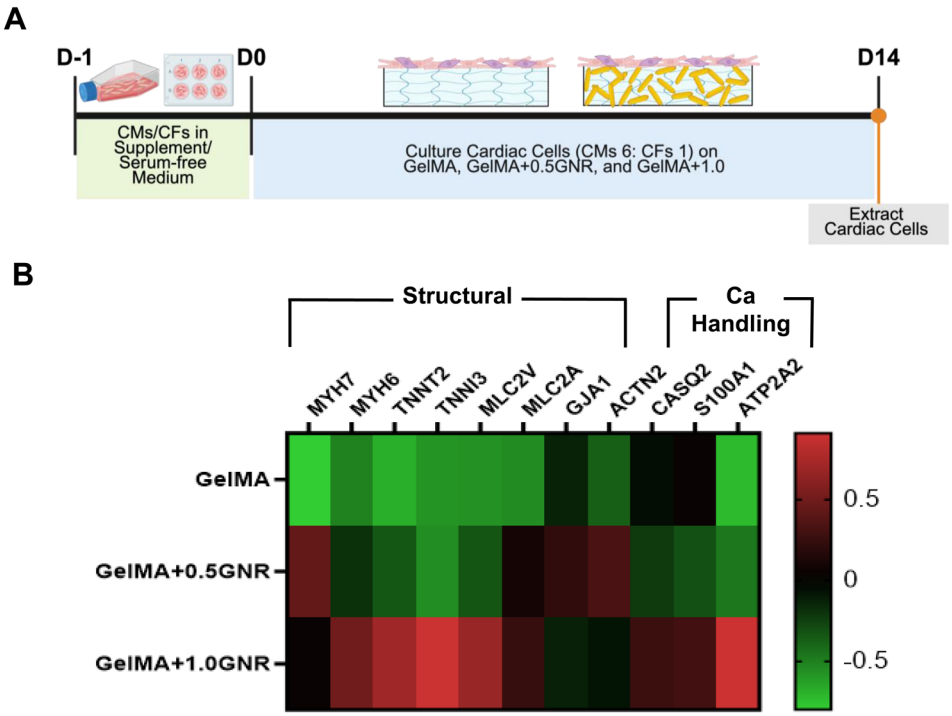

Fig. 6 Gene expression analysis. (A) Schematic workflow of gene expression analysis. The cardiac cells were exposed to a supplement free medium for 24 h before culturing the cells on the GelMA-GNR hydrogel. A mixture of CMs and CFs (6 : 1 ratio) was cultured on GelMA-GNR for 14 days. The GelMA group was used as a control for gene expression normalization. On day 14 of culture, cardiac cells were collected and lysed for gene expression analysis (created with BioRender). (B) Heatmap of RT-qPCR.

3.7 Spontaneous beating behavior analysis

To explore the impact of ETHs on cardiac tissue-level function, electrophysiological behavior of the cardiac tissues, such as interbeat interval variability (IIV), beats per minute (BPM), relaxation time, and contraction amplitude were assessed. Initially, the spontaneous beating signals of the tissues from real-time videos on days 7 and 14 of culture were taken for analysis (Supplementary Video 1–6†). All the real-time videos were processed *via* MUSCLEMOTION for quantification analysis.[44,45] Consistent signals in repetitive beating were observed across all samples (Fig. 7A). While there were no statistically significant differences, there was an overall increase in BPM on day 14 in all samples (Fig. 7B). Relaxation time refers to the period during which the myocardium relaxes after contraction. The quantified data of relaxation time indicated a general decrease on all experimental samples on day 14 (Fig. 7C). Contraction amplitude measured the magnitude or strength of the heart's muscle contraction, which demonstrated a slight decrease in magnitude for all conditions (Fig. 7D). Additionally, quantified data of IIV which evaluates the synchronicity of beating tissues on each scaffold had no significant differences among all experimental conditions (Fig. 7E). Given the absence of significant differences in spontaneous beating characteristics of the tissues, further analyses were performed to determine whether cardiac tissues formed on GelMA-GNR hydrogels, differentially responded to external electrical stimulation through optical mapping.

3.8 Electrophysiological analysis of EHTs through optical mapping

With our custom-made optical mapping system, we were able to acquire the membrane potential signals from the EHTs. The acquired signals were then represented in the form of activation maps to facilitate the visualization, evaluation, and analysis of the electrophysiological properties of the EHTs. In order to evaluate only samples that were physiologically relevant for future *in vivo* applications, a discrimination criterion for samples with low CV was stablished. The CV cutoff was determined at 8 cm s^{-1}, based on the lowest CV values for human heart found in recently published data.[47] Therefore, the samples that presented CV < 8 cm s^{-1}, and their corresponding APD50 and APD80, were not included in the statistical analysis.

The analyzed groups showed CVs values ranging from 10.31 to 17.11 cm s^{-1} (Table S3†). We did not find any significant difference between the control group (GelMA) and the EHTs that contain GNRs (GelMA+0.5GNR and GelMA+1.0GNR) (Fig. 8A). However, row Z-scores showed a trend for higher CV in the GelMA+0.5GNR at lower stimulation frequencies (Fig. 8B). We also found that only APD50 at 2.5 Hz of external electrical stimulation was significantly higher (p-value = 0.0067) for the GelMA+0.5GNR group (Fig. 9A). For the rest of the comparisons for APD50 and APD80 values, we did not find any significant differences (Fig. 9A and B, respectively, and Tables S4 and S5†). Additionally, row Z-scores heatmaps show a trend for higher APD50 and APD80 for the groups containing GNRs (Fig. 9C and D).

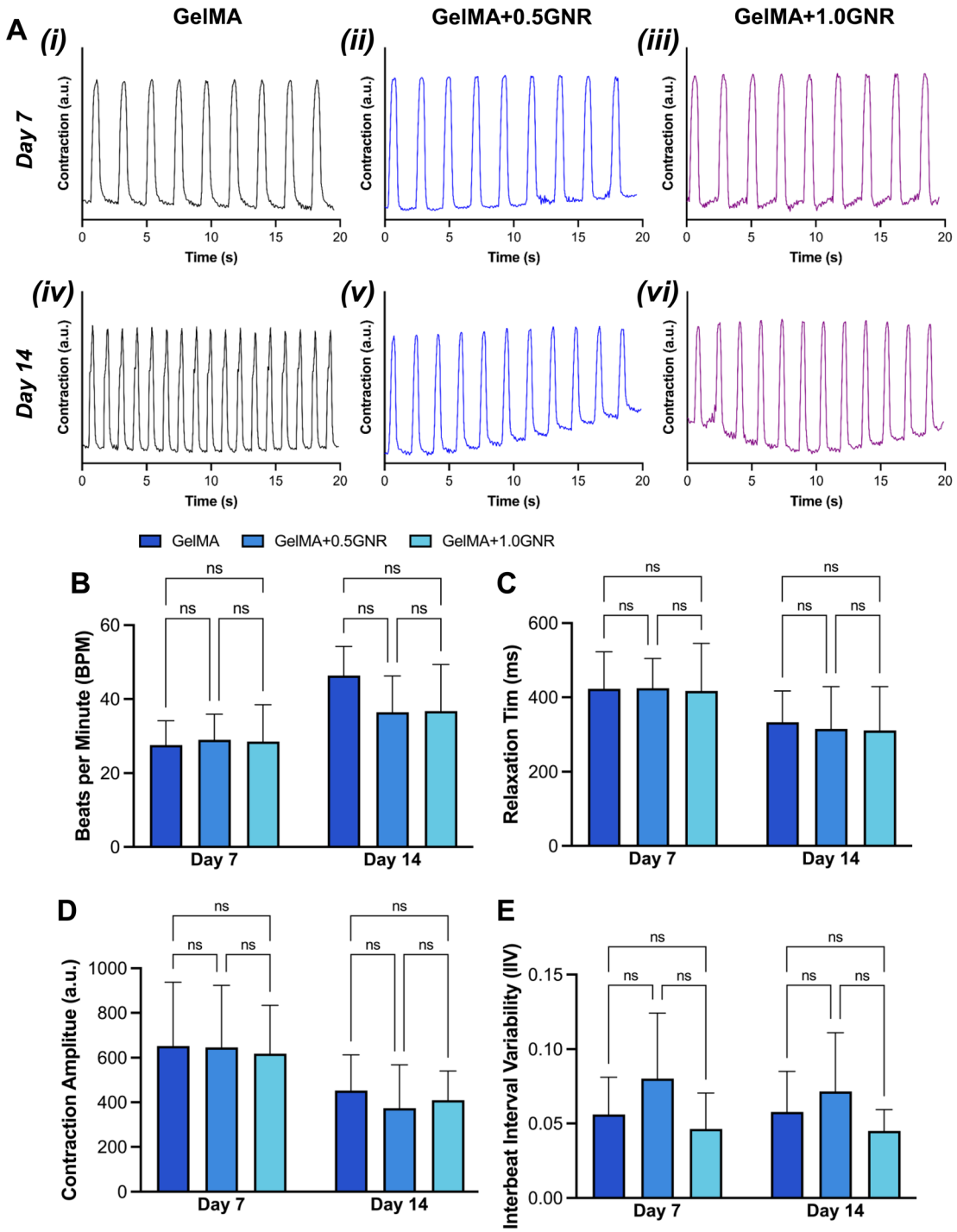

Fig. 7 Spontaneous beating behavior analysis. (A) Representative spontaneous contractility signal graphs of cardiac tissues formed on GelMA (i and iv), GelMA+0.5GNR (ii and v), and GelMA+1.0GNR (iii and vi) on day 7 and 14. Spontaneous (B) beats per minute, (C) relaxation time, (D) contraction amplitude, and (E) interbeat interval variability for all experimental conditions at day 7 and 14 (two-way ANOVA with a Tukey's posthoc test, $n = 4$). Data was expressed as mean ± standard deviation. Ns (not significant).

4. Discussion

In this study, we developed EHTs developed by co-culturing gene-edited cardiomyocytes (hiPSC-CCND2^{OE}CMs) and hiPSC-CFs in a 6 : 1 ratio on electrically conductive GNR-embedded GelMA hydrogels (*i.e.* GelMA-GNR). It has been shown that the presence of GNRs in GelMA hydrogels enhances cell retention, cell-to-cell signaling, and tissue organization.[28–30] Additionally, the maturation of the sarcomeric structure of wild-type hiSPC-CMs has been attributed to the inclusion of GNRs in GelMA hydrogels.[48] Thus, GelMA-GNRs hydrogels are a suitable platform for the fabrication of EHTs, showing improved

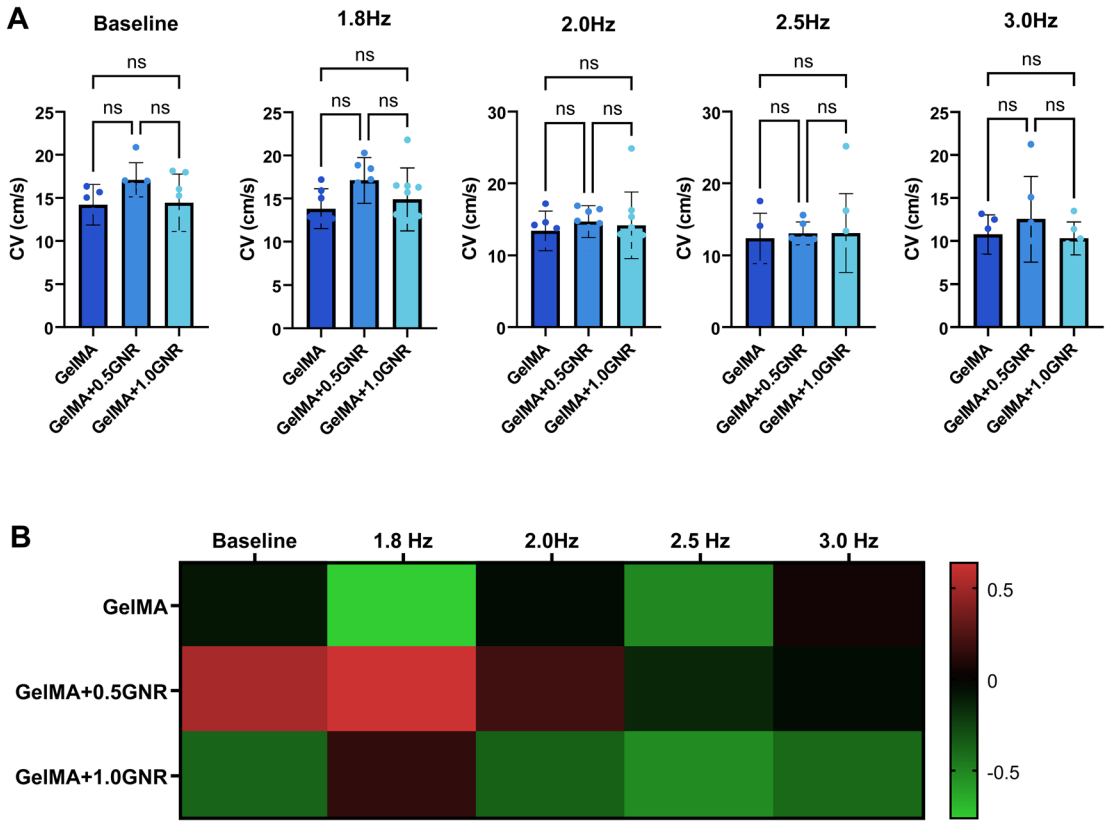

Fig. 8 Conduction velocity of EHTs. (A) Conduction velocity of the EHTs for each specific electrical stimulation frequency, calculated from EHTs activation maps. Each datapoint represents an analyzed sample (One-way ANOVA with Tukey's post hoc test, ns: p-value>0.05). (B) Heatmap for conduction velocity Z-scores. A trend for higher CV of the EHTs containing GNRs is shown.

functionality when compared with pristine or non-electroconductive GelMA EHTs. Thus, this model was designed to evaluate the synergistic potential of electrically conductive biomaterials and gene-edited CMs in promoting functional development of the EHTs. GelMA has been widely explored in regenerative medicine due to its biocompatibility, low immunogenicity, tunable mechanical properties, and ability to support cellular proliferation.[49,50] Furthermore, the incorporation of GNRs enhances the structural integrity of the GelMA matrix through electrostatic interactions, reinforcing the scaffold's stability and potentially improving its biomechanical and electrical properties.[28,51] Notably, previous studies have demonstrated that incorporating nanomaterials such as GNRs into GelMA matrices significantly enhances their mechanical resilience of hydrogel.[28,30,51] The electrostatic interactions between GelMA and GNRs reinforce the polymer network, improving its stiffness and resistance to deformation under stress. In addition to their mechanical role, GNRs contribute electrical conductivity values in the range of the native myocardial tissue. This has motivated their use in the development of electrically conductive, bioactive hydrogels for MI therapy.[28,52–54] In our work, the absence of hydrogel structural collapse, along with the observed positive cellular outcomes suggests that the mechanical stability of the GelMA-GNR hydrogel was sufficient to support hiPSC-CCND2^{OE}CMs over the experimental timeframe. These combined properties highlight GelMA-GNR as a promising scaffold for cardiac tissue engineering.

A fundamental requirement for biomaterials in cardiac tissue engineering is cell survival.[55] Our results demonstrated that incorporating GNRs at concentrations of 0.5 and 1.0 mg mL^{-1} into GelMA hydrogels did not compromise cell viability, supporting the feasibility of GelMA-GNR as a suitable biomaterial for EHTs. Additionally, spontaneous beating behavior remained unchanged with GNR incorporation, indicating that GNRs did not interfere with the intrinsic excitability and pacemaker activity of cardiomyocytes. This suggests that the GelMA-GNR scaffold provided a supportive microenvironment without disrupting ion channel function, electrical excitability, or contraction dynamics, all of which are crucial for cardiac tissue functionality.

To further characterize the morphological and phenotypic changes in EHTs, immunostaining for F-actin and integrin β1 was performed. Notably, hiPSC-CCND2^{OE}CMs seeded on GelMA-GNR hydrogels exhibited a more clustered morphology compared to those cultured on GelMA alone. This increased clustering suggests that GNRs influence cell adhesion dynamics, potentially enhancing intercellular interactions and promoting tissue organization and structural formation. This effect may arise from modifications in electroconductivity,

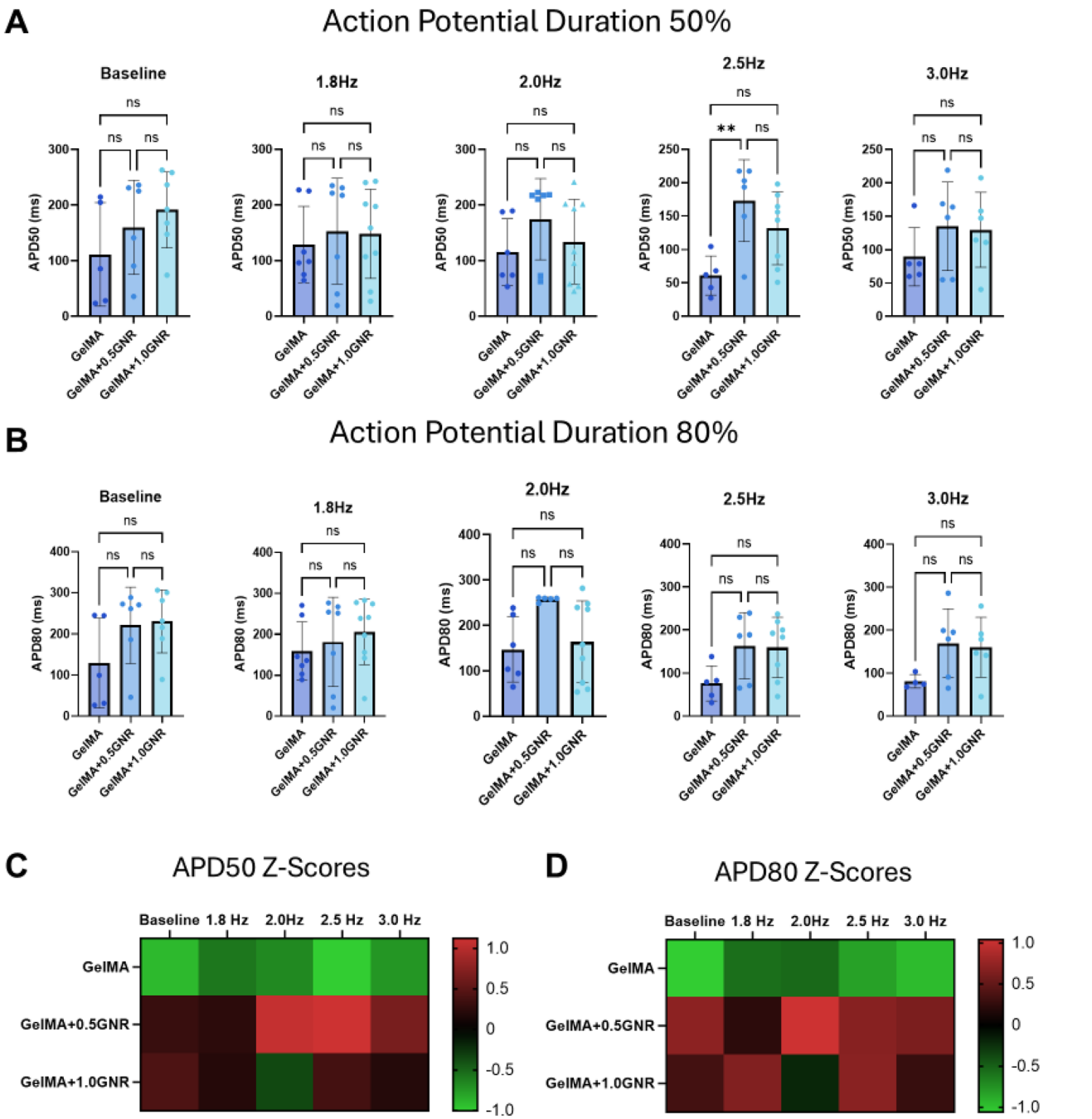

Fig. 9 Action potential duration of EHTs. EHTs action potential duration at (A) 50% repolarization (APD50) and (B) 80% repolarization (APD80). APD50 and APD80 calculated from the activation maps. Each datapoint represents an analyzed sample (One-way ANOVA with Tukey's post hoc test, ns: p-value > 0.05). Heatmaps for (C) APD50 Z-scores and (D) APD80 Z-scores.

biochemical signaling, or potentially biophysical cues within the substrate due to presence of GNRs, all of which could favor cell–cell adhesion over cell-substrate adhesion. Importantly, the enhanced CMs clustering in GelMA-GNR was accompanied by a significant increase in Cx43 expression, suggesting improved intercellular electrical coupling. Cx43 is a crucial gap junction protein responsible for rapid electrical signal propagation and synchronized contraction in cardiac tissue.[56] The upregulation of Cx43 suggests that GNRs not only promote cell aggregation but also facilitate syncytium formation, which is essential for effective myocardial regeneration.[57,58] It has been demonstrated that GNRs also contribute to tissue engineering by introducing nanoscale topographical features.[30,31] While this does not directly affect the electrical propagation, it can help with enhanced cell attachment and cell-to-cell coupling. This interpretation aligns with our findings of higher Cx43 expression in the GelMA+GNR groups.

Previously, hiPSC-CCND2^{OE}CMs were shown to exhibit enhanced proliferation in infarcted mouse hearts.[46] To assess whether hiPSC-CCND2^{OE}CMs maintain their proliferative capacity when cultured on GelMA-GNR hydrogels, EHTs were stained for ki67, a marker of active proliferation. Ki67 staining revelaed evidence of CMs proliferation, indicating that the incorporation of GNRs did not hinder the proliferative potential of hiPSC-CCND2^{OE}CMs.

To further explore the effects of the GelMA-GNR hydrogels on gene expression profiles of hiPSC-CCND2^{OE}CMs, we performed qPCR of cells cultured on GelMA, GelMA+0.5GNR, and GelMA+1.0GNR for 14 days. These gene expression trends provide further insight into how the structural and material properties of the GelMA-GNR hydrogels may influence cardiomyocyte behavior at the molecular level. Although RT-qPCR did not reveal statistically significant differences, the row heatmap analysis demonstrates a clear pattern of upregulation in genes associated with cardiac structure and calcium handling, particularly in the GelMA+1.0GNR condition. This suggests that increased GNR concentration may promote a more mature or activated transcriptional profile in engineered cardiac tissues. The observed gene expression shifts may reflect enhanced structural organization and electromechanical coupling, aligning with prior immunofluorescence findings. Collectively, these data support the potential of GNR-integrated GelMA hydrogels to modulate the transcriptional landscape of hiPSC-CCND2^{OE}CMs and improve EHT maturation moderately.

Optical mapping has been used as a powerful tool for representing the electrical activity of cardiac tissues.[59,60] They allow for high spatiotemporal resolution analysis and help with the detection of wave propagation patterns and the calculation of CV, APD, among other electrophysiological parameters. While we did not find any significant differences among experimental groups, there is a trend that suggests that the GNRs may have a positive effect on higher CV. One of the primary motivations for incorporating GNRs into the GelMA scaffold was to improve electrical conductivity. APD50 and APD80 are within range of what other authors have reported for stem cell-derived EHTs.[61] The trend for increased APD50 and APD80 needs to be further investigated by analyzing not only the APDs, but also the action potentials signal geometry (*i.e.*, phase 0 to phase 4 separately), the expression of the specific ion channels related to each action potential phase,[62] and the cellular contraction force for each of the experimental groups.

Ultimately, the goal of developing EHTs is their successful integration with native myocardium. While we understand that CV is a complex parameter for anisotropic tissues, we believe that our initial discrimination criterium of CV <8 cm s^{-1} will allow to have EHTs that better mimic the electrophysiological features of the native myocardium and therefore, will facilitate their integration with the native myocardium. This criterium was based in recently published data that reports CV measured with modern acquisition methods,[47] similar to our optical mapping protocol. In our future studies in this regard, we aim to further optimize hydrogel materials, GNRs concentration and cell culture (*i.e.*, 3D encapsulation instead of 2d seeding) to further enhance the functionality and electrophysiological response of the EHTs.

While GelMA-GNR patches demonstrated biocompatibility and enhanced cellular organization, no statistically significant differences were observed in CV, APD, or the expression of calcium-handling and ultrastructural genes compared to the GelMA-only group. One potential explanation is overexpression of Cyclin D2 in CMs. Cyclin D2 is a key regulator of cell cycle progression, and its overexpression may force CMs into a proliferative state, counteracting the natural maturation process.[46] Mature CMs exit the cell cycle to prioritize structural, metabolic, and electrophysiological specialization, which is essential for functional myocardium.[63] However, CCND2 overexpression reactivates the cell cycle, potentially preventing the complete development of mature sarcomere organization, hypertrophic growth, and the metabolic shift from glycolysis to oxidative phosphorylation—hallmarks of cardiomyocyte maturation.[64–66] Additionally, proliferative CMs may retain an immature ion channel profile, potentially affecting electrical stability and contractile function. The competition between proliferation-associated pathways (*e.g.*, CDK4/6 activation, Rb phosphorylation) and differentiation signals (*e.g.*, MEF2, SRF, and PGC-1α signaling) reinforces a fetal-like, immature phenotype.[67–69] While CCND2 overexpression is advantageous for enhancing CMs regeneration, strategies to transiently regulate its expression may be necessary to balance proliferation with functional maturation, ensuring the development of fully integrated, contractile myocardial tissue.

Taken together, our findings in this initial stage study suggest that GelMA-GNR hydrogels provide a promising scaffold for the formation EHTs, demonstrating biocompatibility, enhanced cellular organization, improved intercellular coupling and enhanced function. However, the lack of statistically significant differences in ultrastructural gene expression as well as electrophysiological response of the tissue compared to GelMA alone (without GNRs) highlights the complex interplay between biomaterial properties and cellular behavior. In addition, our results underscore the need for further optimization of hiPSC-CCND2^{OE}CM maturation strategies to ensure that engineered tissues achieve both regenerative capacity and functional integration with the native myocardium.

5. Conclusion

This study presents the development of a novel EHT platform by integrating gene-edited hiPSC-CCND2^{OE}CM and cardiac fibroblasts within a GelMA-GNR hydrogel scaffold. Our data demonstrate that the GelMA-GNR hydrogels are biocompatible, structurally stable, and supportive of cardiomyocyte viability, and proliferation. The inclusion of GNRs enhanced cell–cell coupling, as evidenced by increased Cx43 expression, and modestly influenced the electrophysiological and gene expression profiles associated with cardiomyocyte maturation. Although the improvements in conduction velocity, action potential duration, and structural gene expression did not reach statistical significance, observed trends and enhanced tissue organization suggest that GNRs may positively modulate the

electrophysiological microenvironment and cellular architecture. These findings also reveal that the persistent proliferative phenotype induced by CCND2 overexpression may limit full maturation of hiPSC-CMs, underscoring the need for temporally regulated gene expression strategies in regenerative applications. Together, these results highlight the potential of GelMA-GNR scaffolds to support the development of functional and regenerative EHTs. Future optimization of biomaterial properties, and cell-intrinsic maturation pathways will be critical to achieve robust functional integration with host myocardium and improve the clinical potential of engineered cardiac tissues.

Data availability

The data supporting this article have been included as part of the ESI.†

Author contributions

MJ initiated the project, conducted experiments, acquired and analyzed data, and wrote the manuscript. YS, AP, YS, and KN conducted experiments, acquired and analyzed data, and wrote the manuscript. MN and WZ designed research studies, wrote the manuscript, and handled finance.

Conflicts of interest

The authors have declared that no conflict of interest exists.

Acknowledgements

This work is supported by NIH NHLBI grants (R01 HL172784 to MN and WZ, and R01 HL142627, HL156855, and HL162747 to WZ), and the AHA postdoctoral fellowship award (24POST1196653 to APG).

References

1 L. Lu, M. Liu, R. Sun, Y. Zheng and P. Zhang, *Cell Biochem. Biophys.*, 2015, **72**, 865–867.
2 A. Uygur and R. T. Lee, *Dev. Cell*, 2016, **36**, 362–374.
3 C. Ambastha, G. J. Bittle, D. Morales, N. Parchment, P. Saha, R. Mishra, S. Sharma, A. Vasilenko, M. Gunasekaran and M. T. Al-Suqi, *Transl. Pediatr.*, 2018, **7**, 176.
4 J. J. Chong, X. Yang, C. W. Don, E. Minami, Y.-W. Liu, J. J. Weyers, W. M. Mahoney, B. Van Biber, S. M. Cook and N. J. Palpant, *Nature*, 2014, **510**, 273–277.
5 J. Zhang, W. Zhu, M. Radisic and G. Vunjak-Novakovic, *Circ. Res.*, 2018, **123**, 244–265.
6 M. Qasim, P. Arunkumar, H. M. Powell and M. Khan, *Life Sci.*, 2019, **229**, 233–250.
7 M. P. Prabhakaran, D. Kai, L. Ghasemi-Mobarakeh and S. Ramakrishna, *Biomed. Mater.*, 2011, **6**, 055001.
8 C. Williams, E. Budina, W. L. Stoppel, K. E. Sullivan, S. Emani, S. M. Emani and L. D. Black III, *Acta Biomater.*, 2015, **14**, 84–95.
9 K. L. Christman, A. J. Vardanian, Q. Fang, R. E. Sievers, H. H. Fok and R. J. Lee, *J. Am. Coll. Cardiol.*, 2004, **44**, 654–660.
10 S. Rinkevich-Shop, N. Landa-Rouben, F. H. Epstein, R. Holbova, M. S. Feinberg, O. Goitein, T. Kushnir, E. Konen and J. Leor, *J. Cardiovasc. Pharmacol. Ther.*, 2014, **19**, 470–480.
11 W. Hu, C. Yang, X. Guo, Y. Wu, X. J. Loh, Z. Li, Y.-L. Wu and C. Wu, *Gels*, 2022, **8**, 423.
12 T. Hao, J. Li, F. Yao, D. Dong, Y. Wang, B. Yang and C. Wang, *ACS Nano*, 2017, **11**, 5474–5488.
13 B. Deng, L. Shen, Y. Wu, Y. Shen, X. Ding, S. Lu, J. Jia, J. Qian and J. Ge, *J. Biomed. Mater. Res., Part A*, 2015, **103**, 907–918.
14 A. Navaei, D. Truong, J. Heffernan, J. Cutts, D. Brafman, R. W. Sirianni, B. Vernon and M. Nikkhah, *Acta Biomater.*, 2016, **32**, 10–23.
15 S. Dobner, D. Bezuidenhout, P. Govender, P. Zilla and N. Davies, *J. Card. Failure*, 2009, **15**, 629–636.
16 L. M. Monteiro, F. Vasques-Nóvoa, L. Ferreira, P. Pinto-do-Ó and D. S. Nascimento, *npj Regener. Med.*, 2017, **2**, 9.
17 S. He, J. Wu, S.-H. Li, L. Wang, Y. Sun, J. Xie, D. Ramnath, R. D. Weisel, T. M. Yau and H.-W. Sung, *Biomaterials*, 2020, **258**, 120285.
18 H. Esmaeili, A. Patino-Guerrero, M. Hasany, M. O. Ansari, A. Memic, A. Dolatshahi-Pirouz and M. Nikkhah, *Acta Biomater.*, 2022, **139**, 118–140.
19 J. Lee, V. Manoharan, L. Cheung, S. Lee, B.-H. Cha, P. Newman, R. Farzad, S. Mehrotra, K. Zhang and F. Khan, *ACS Nano*, 2019, **13**, 12525–12539.
20 S. R. Shin, S. M. Jung, M. Zalabany, K. Kim, P. Zorlutuna, S. b. Kim, M. Nikkhah, M. Khabiry, M. Azize and J. Kong, *ACS Nano*, 2013, **7**, 2369–2380.
21 S. R. Shin, C. Zihlmann, M. Akbari, P. Assawes, L. Cheung, K. Zhang, V. Manoharan, Y. S. Zhang, M. Yüksekkaya and K. t. Wan, *Small*, 2016, **12**, 3677–3689.
22 S. R. Shin, B. Aghaei-Ghareh-Bolagh, X. Gao, M. Nikkhah, S. M. Jung, A. Dolatshahi-Pirouz, S. B. Kim, S. M. Kim, M. R. Dokmeci and X. Tang, *Adv. Funct. Mater.*, 2014, **24**, 6136–6144.
23 M. Kharaziha, S. R. Shin, M. Nikkhah, S. N. Topkaya, N. Masoumi, N. Annabi, M. R. Dokmeci and A. Khademhosseini, *Biomaterials*, 2014, **35**, 7346–7354.
24 X.-P. Li, K.-Y. Qu, F. Zhang, H.-N. Jiang, N. Zhang, C. Nihad, C.-M. Liu, K.-H. Wu, X.-W. Wang and N.-P. Huang, *J. Mater. Chem. B*, 2020, **8**, 7213–7224.
25 A. Patino-Guerrero, H. Esmaeili, R. Q. Migrino and M. Nikkhah, *RSC Adv.*, 2023, **13**, 16985–17000.
26 C.-W. Hsiao, M.-Y. Bai, Y. Chang, M.-F. Chung, T.-Y. Lee, C.-T. Wu, B. Maiti, Z.-X. Liao, R.-K. Li and H.-W. Sung, *Biomaterials*, 2013, **34**, 1063–1072.
27 C. M. Cobley, J. Chen, E. C. Cho, L. V. Wang and Y. Xia, *Chem. Soc. Rev.*, 2011, **40**, 44–56.
28 A. Navaei, H. Saini, W. Christenson, R. T. Sullivan, R. Ros and M. Nikkhah, *Acta Biomater.*, 2016, **41**, 133–146.
29 A. Navaei, N. Moore, R. T. Sullivan, D. Truong, R. Q. Migrino and M. Nikkhah, *RSC Adv.*, 2017, **7**, 3302–3312.

30 A. Navaei, K. R. Eliato, R. Ros, R. Q. Migrino, B. C. Willis and M. Nikkhah, *Biomater. Sci.*, 2019, **7**, 585–595.
31 H. Esmaeili, A. Patino-Guerrero, R. A. Nelson Jr, N. Karamanova, T. M. Fisher, W. Zhu, F. Perreault, R. Q. Migrino and M. Nikkhah, *ACS Biomater. Sci. Eng.*, 2024, **10**, 2351–2366.
32 H. Esmaeili, Y. Zhang, K. Ravi, K. Neff, W. Zhu, R. Q. Migrino, J. G. Park and M. Nikkhah, *Biomaterials*, 2025, 123275.
33 C. Fan, V. G. Fast, Y. Tang, M. Zhao, J. F. Turner, P. Krishnamurthy, J. M. Rogers, M. T. Valarmathi, J. Yang, W. Zhu and J. Zhang, *J. Mol. Cell. Cardiol.*, 2019, **137**, 25–33.
34 D. Loessner, C. Meinert, E. Kaemmerer, L. C. Martine, K. Yue, P. A. Levett, T. J. Klein, F. P. Melchels, A. Khademhosseini and D. W. Hutmacher, *Nat. Protoc.*, 2016, **11**, 727–746.
35 B. Nikoobakht and M. A. El-Sayed, *Chem. Mater.*, 2003, **15**, 1957–1962.
36 W. Tong, M. J. Walsh, P. Mulvaney, J. Etheridge and A. M. Funston, *J. Phys. Chem. C*, 2017, **121**, 3549–3559.
37 L. Scarabelli, A. Sánchez-Iglesias, J. Pérez-Juste and L. M. Liz-Marzán, *J. Phys. Chem. Lett.*, 2015, **6**, 4270–4279.
38 Y. Son, P. Li, D. Ortega, H. Qiu, H. Prachyl, M. Yang and W. Zhu, *Small Methods*, 2024, 2301764, DOI: **10.1002/smtd.202301764**.
39 J. Joshi, B. Xu, M. Rubart, Y. Chang, X. Bao, H. P. Chaliki, L. R. Scott and W. Zhu, *Cells*, 2022, **11**, 951.
40 D. J. Richards, Y. Tan, R. Coyle, Y. Li, R. Xu, N. Yeung, A. Parker, D. R. Menick, B. Tian and Y. Mei, *Nano Lett.*, 2016, **16**, 4670–4678.
41 A. A. Benbuk, H. Esmaeili, S. Liu, A. Patino-Guerrero, R. Q. Migrino, J. Chae, M. Nikkhah and J. Blain Christen, *ACS Sens.*, 2022, **7**, 3287–3297.
42 J. Veldhuizen, R. Chavan, B. Moghadas, J. G. Park, V. D. Kodibagkar, R. Q. Migrino and M. Nikkhah, *Biomaterials*, 2022, **281**, 121336.
43 J. Veldhuizen and M. Nikkhah, *J. Visualized Exp.*, 2021, **172**, e62539.
44 B. J. van Meer, L. Sala, L. G. Tertoolen, G. L. Smith, F. L. Burton and C. L. Mummery, *Curr. Protoc. Hum. Genet.*, 2018, **99**, e67.
45 L. Sala, B. J. Van Meer, L. G. Tertoolen, J. Bakkers, M. Bellin, R. P. Davis, C. Denning, M. A. Dieben, T. Eschenhagen and E. Giacomelli, *Circ. Res.*, 2018, **122**, e5–e16.
46 W. Zhu, M. Zhao, S. Mattapally, S. Chen and J. Zhang, *Circ. Res.*, 2018, **122**, 88–96.
47 Z. Fu, R. Dong, H. Zheng, Z. Wang, B. Cao, J. Bai, M. Ma, Z. Song, F. Pan and L. Xia, *Mol. Rev. Cardiovasc. Med.*, 2024, **25**, 364.
48 H. Esmaeili, A. Patino-Guerrero, R. A. Nelson Jr, N. Karamanova, T. M. Fisher, W. Zhu, F. Perreault, R. Q. Migrino and M. Nikkhah, *ACS Biomater. Sci. Eng.*, 2024, **10**, 2351–2366.
49 L. Xiang and W. Cui, *J. Leather Sci. Eng.*, 2021, **3**, 3.
50 Y. Piao, H. You, T. Xu, H.-P. Bei, I. Z. Piwko, Y. Y. Kwan and X. Zhao, *Eng. Regener.*, 2021, **2**, 47–56.
51 A. G. Kurian, R. K. Singh, K. D. Patel, J.-H. Lee and H.-W. Kim, *Bioact. Mater.*, 2022, **8**, 267–295.
52 J. Chen, X. Han, J. Deng, J. Zhang, L. Li, J. Ni, Y. Huang, X. Xie, S. Chen and L. Ke, *Chem. Eng. J.*, 2021, **413**, 127423.
53 A. Jahangiri-Manesh, M. Mousazadeh, S. Taji, A. Bahmani, A. Zarepour, A. Zarrabi, E. Sharifi and M. Azimzadeh, *Pharmaceutics*, 2022, **14**, 664.
54 P. Baei, S. Jalili-Firoozinezhad, S. Rajabi-Zeleti, M. Tafazzoli-Shadpour, H. Baharvand and N. Aghdami, *Mater. Sci. Eng., C*, 2016, **63**, 131–141.
55 D. Zhang, R. He, Y. Qu, C. He and B. Chu, *MedComm: Biomater. Appl.*, 2024, **3**, e103.
56 A. Rodríguez-Sinovas, J. A. Sánchez, L. Valls-Lacalle, M. Consegal and I. Ferreira-González, *Int. J. Mol. Sci.*, 2021, **22**(9), 4413.
57 T. A. B. van Veen, H. V. M. van Rijen and T. Opthof, *Cardiovasc. Res.*, 2001, **51**, 217–229.
58 A. R. Soares, T. Martins-Marques, T. Ribeiro-Rodrigues, J. V. Ferreira, S. Catarino, M. J. Pinho, M. Zuzarte, S. Isabel Anjo, B. Manadas, J. P. G. Sluijter, P. Pereira and H. Girao, *Sci. Rep.*, 2015, **5**, 13243.
59 J. I. Laughner, F. S. Ng, M. S. Sulkin, R. M. Arthur and I. R. Efimov, *Am. J. Physiol. Renal Physiol.*, 2012, **303**, H753–H765.
60 C. O'Shea, S. N. Kabir, A. P. Holmes, M. Lei, L. Fabritz, K. Rajpoot and D. Pavlovic, *Int. J. Biochem. Cell Biol.*, 2020, **126**, 105804.
61 G. Campostrini, L. M. Windt, B. J. van Meer, M. Bellin and C. L. Mummery, *Circ. Res.*, 2021, **128**, 775–801.
62 H. Tani and S. Tohyama, *Front. Cell Dev. Biol.*, 2022, **10**, 855763.
63 E. Karbassi, A. Fenix, S. Marchiano, N. Muraoka, K. Nakamura, X. Yang and C. E. Murry, *Nat. Rev. Cardiol.*, 2020, **17**, 341–359.
64 A. M. Pettinato, F. A. Ladha and J. T. Hinson, *Curr. Cardiol. Rep.*, 2022, **24**, 623–630.
65 R. A. Poolman and G. Brooks, *J. Mol. Cell. Cardiol.*, 1998, **30**, 2121–2135.
66 G. D. Lopaschuk and J. S. Jaswal, *J. Cardiovasc. Pharmacol.*, 2010, **56**, 130–140.
67 Y. J. Choi and L. Anders, *Oncogene*, 2014, **33**, 1890–1903.
68 V. Di Stefano, M. Giacca, M. C. Capogrossi, M. Crescenzi and F. Martelli, *J. Biol. Chem.*, 2011, **286**, 8644–8654.
69 E. Perdiguero, P. Sousa-Victor, E. Ballestar and P. Muñoz-Cánoves, *Epigenetics*, 2009, **4**, 541–550.